CHAPTER W12

Metals and Alloys

A variety of theoretical tools is available for the study of metallic solids. Electronic band-structure methods include the augmented plane wave (APW) method, the orthogonalized plane wave (OPW) method, the Green function [Korringer, Kohn, and Rostoker (KKR)] method, the pseudopotential method, and the cellular (Wigner–Seitz) method. These approaches are discussed in solid-state physics textbooks (e.g., Fletcher or Ashcroft and Mermin). These methods all rely on the perfect periodicity of the solid and utilize Bloch's theorem to limit the focus of attention to a unit cell. They are not directly applicable to disordered alloys or solids with impurities or defects.

Quantum-chemistry calculations can be done for clusters of finite size, but the computational time grows rapidly as the size of the cluster is increased, making such calculations impractical for the study of large collections of atoms with present-day computers.

The next three sections introduce methods that have found some utility in describing realistic solids: the density-functional method, the embedded-atom method, and the tight-binding approximation. Although lacking the accuracy of the band-structure or quantum-chemistry computations, they are nevertheless useful in studying large-scale systems, are relatively simple to implement on the computer, and are, for many purposes, adequate.

W12.1 Density-Functional Theory

Density-functional theory is a method currently being used to obtain a theoretical understanding of metals, metallic alloys, surfaces of metals, and imperfections in metals. The method is a natural outgrowth of the Thomas–Fermi method introduced in Chapter 7 of the textbook.[†] It is based on the observation by Hohenberg and Kohn that all the ground-state properties of a many-body quantum-mechanical system of electrons may be obtained from a knowledge of the electron density, $n(\mathbf{r})$. They proved that $n(\mathbf{r})$ determines the potential $V(\mathbf{r})$ that the electrons move in, up to an insignificant additive constant. Furthermore, an energy functional $E[n]$ may be constructed and it may be shown to attain its minimum value when the correct $n(\mathbf{r})$ is employed.

The uniqueness proof is based on the minimum principle from quantum mechanics. Begin by noting that if the potential energy function $V(\mathbf{r})$ were known, one could solve

[†] The material on this home page is supplemental to *The Physics and Chemistry of Materials* by Joel I. Gersten and Frederick W. Smith. Cross-references to material herein are prefixed by a "W"; cross-references to material in the textbook appear without the "W."

the Schrödinger equation and obtain the electron density $n(\mathbf{r})$. If there were two different potentials $V(\mathbf{r})$ and $V'(\mathbf{r})$ leading to the same $n(\mathbf{r})$, the Schrödinger equation could be solved for each potential and the respective ground-state wavefunctions ψ and ψ' would be determined. By the minimum principle, the ground-state energy obeys the inequality

$$E = \langle\psi|(T+V)|\psi\rangle < \langle\psi'|(T+V)|\psi'\rangle = \langle\psi'|(T+V')|\psi'\rangle + \langle\psi'|(V-V')|\psi'\rangle$$
$$= E' + \langle\psi'|(V-V')|\psi'\rangle = E' + \int n(\mathbf{r})[V(\mathbf{r}) - V'(\mathbf{r})]\,d\mathbf{r}. \tag{W12.1}$$

Repeating the argument with the primed and unprimed variables interchanged leads to $E' < E + \int n(\mathbf{r})[V'(\mathbf{r}) - V(\mathbf{r})]\,d\mathbf{r}$. Adding the two inequalities leads to the contradiction $E + E' < E' + E$. Q.E.D.

The energy of the system is written in the form

$$E[n] = \int n(\mathbf{r}) \left[\frac{3}{5}E_F(\mathbf{r})\right] d\mathbf{r} + \int n(\mathbf{r})V(\mathbf{r})\,d\mathbf{r} + E_{ii}$$
$$+ \frac{1}{2}\frac{e^2}{4\pi\epsilon_0}\int d\mathbf{r}\int d\mathbf{r}'\frac{n(\mathbf{r})n(\mathbf{r}')}{|\mathbf{r}-\mathbf{r}'|} + E_{\mathrm{xc}}[n]. \tag{W12.2}$$

Here $E_F = \hbar^2 k_F^2/2m$, where $k_F(\mathbf{r}) = [3\pi^2 n(\mathbf{r})]^{1/3}$ is a local Fermi wave vector, and $V(\mathbf{r})$ is the potential due to the ions. The first four terms are the kinetic energy, the energy of interaction of the electrons with the ions, the ion–ion interaction, and the Coulomb repulsion energy of the electrons. The quantity E_{xc} is the energy arising from exchange and correlation effects. The variational problem may be reduced to the solution of a set of partial-differential equations called the Kohn–Sham equations. These are of the form

$$\left[-\frac{\hbar^2}{2m}\nabla^2 + v_{\mathrm{eff}}(\mathbf{r}) - E_j\right]\psi_j(\mathbf{r}) = 0, \tag{W12.3}$$

where $E_{xc}[n] = \int n\epsilon_{xc}\,d\mathbf{r}$ and

$$v_{\mathrm{eff}}(\mathbf{r}) = V(\mathbf{r}) + \frac{e^2}{4\pi\epsilon_0}\int\frac{n(\mathbf{r}')}{|\mathbf{r}-\mathbf{r}'|}d\mathbf{r}' + v_{\mathrm{xc}}(\mathbf{r}), \tag{W12.4}$$

$$v_{\mathrm{xc}}(\mathbf{r}) = \frac{\delta E_{\mathrm{xc}}[n(\mathbf{r})]}{\delta n(\mathbf{r})}. \tag{W12.5}$$

The electron density is constructed from the Kohn–Sham wavefunctions as

$$n(\mathbf{r}) = \sum_{j=1}^{N}|\psi_j(\mathbf{r})|^2. \tag{W12.6}$$

In the local-density approximation (LDA) it is assumed that E_{xc} depends only on n and not on its derivatives, and one writes

$$v_{\mathrm{xc}} \approx \frac{d}{dn}(n\epsilon_{\mathrm{xc}}). \tag{W12.7}$$

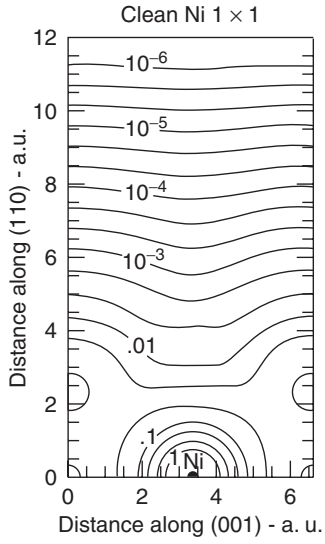

Figure W12.1. Surface-charge density for Ni. Distance is measured in atomic units (a.u.). [Adapted from D. R. Hamann, *Phys. Rev. Lett.*, **46**, 1227 (1981). Copyright 1981 by the American Physical Society.]

Various research groups have presented useful functional forms for $\epsilon_{\rm xc}(n)$. The results of the calculations of $n(\mathbf{r})$ generally compare favorably with experiment or with quantum-chemistry calculations for finite systems. Density-functional theory has also been extended to include corrections involving ∇n terms. An example of calculational results for the surface-charge density of Ni is given in Fig. W12.1.

W12.2 Embedded-Atom Method

The embedded-atom method attempts to calculate the energy of realistic metals by making simplifying assumptions about how atoms interact with each other and with the common sea of electrons. The energy is written as a sum of two terms

$$E = E_{\rm rep} + E_{\rm embed}. \tag{W12.8}$$

The first term is the interatomic-repulsive energy associated with the nuclei and their core electrons. The repulsive energy is given by the sum of pairwise potentials:

$$E_{\rm rep} = \frac{1}{2} \sum_{\substack{i,j \\ i \neq j}} U_{ij}(\mathbf{R}_{ij}). \tag{W12.9}$$

The second term is the interaction of the atoms with the electron gas in which the atoms find themselves embedded. The embedding energy is approximated as the sum of the energies of interaction of each atom with a *uniform* electron gas. The electron density at site i is computed by superimposing the local electronic densities from all

other atoms. Thus

$$E_{\text{embed}} = \sum_i F_i \left[\sum_j {}' n_j(\mathbf{R}_i - \mathbf{R}_j) \right]. \tag{W12.10}$$

The embedding energy, $F_i(n_0)$, is computed using density-functional theory. A point charge ze is placed at the origin. The jellium model is used for the electron gas. The charge density is given by $\rho(\mathbf{r}) = e[n_0 + z\delta(\mathbf{r}) - n(\mathbf{r})]$. Detailed calculations were carried out for a number of elements.† Typical results are presented in Fig. W12.2. Values for the densities at which the minimum occurs and the corresponding well depths are presented in Table W12.1.

Often $F_i(n_0)$ is approximated by a function of the form

$$F_i(n_0) = A_i n_0 - B_i \sqrt{n_0}. \tag{W12.11}$$

The first term corresponds to the effect of the filled shells of the ion. For example, in the inert gases, where all the shells are filled, the embedding energy is observed to grow approximately linearly with the electron density, with a slope given by A_i. The second term arises from the bonding of the valence electrons of the atom with the ambient electrons. If the volume of the embedded atom is Ω, the number of electrons that the atom overlaps with is $N = n_0\Omega$. In a tight-binding description, in which each ambient electron is assigned to a neighboring site, one would could construct a wavefunction as a superposition of the form $|\psi\rangle = (|1\rangle + \cdots + |N\rangle)/\sqrt{N}$, where each term represents a state localized on a given site. The tunneling-matrix element linking the atom to the ith neighbor would be of the form $t = \langle\psi_0|V|i\rangle/\sqrt{N}$. A band whose width is given by $2Nt$ would form. If the state at the bottom of that band is occupied, this would result in a reduction of energy $\Delta E_i = -\langle\psi_0|V|i\rangle\sqrt{N} \equiv -B_i\sqrt{n_0}$. It is interesting to note that the metallic bond is unsaturated (i.e., only part of the band is occupied). If the full band were occupied, the band energy would not be reduced and B_i would be zero.

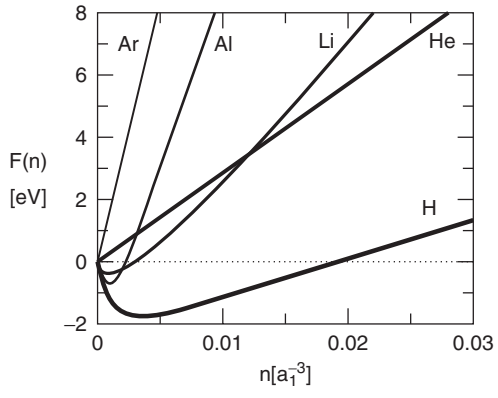

Figure W12.2. Embedding energy as a function of electron density for several elements. Here a_1 is the Bohr radius. [Adapted from M. J. Puska, R. M. Nieminen, and M. Manninen, *Phys. Rev. B*, **24**, 3037 (1981). Copyright 1981 by the American Physical Society.]

† M. J. Puska, R. M. Nieminen, and M. Manninen, *Phys. Rev. B*, **24**, 3037 (1981).

TABLE W12.1 Position and Depth of the Minimum of the Embedding Energy

Atom	n_0 $(a_1^{-3})^a$	$F(n_0)$ (eV)
H	0.0026	−1.8
He	0	—
C	0.0035	−1.8
N	0.0045	−1.4
O	0.0037	−4.1
F	0.0010	−5.1
Ne	0	—
Na	<0.0005	<−0.6
Al	0.0005	−0.2
Cl	0.0005	−4.0

Source: Data from M. J. Puska, R. M. Nieminen, and M. Manninen, *Phys. Rev. B*, **24**, 3037 (1981).

[a] a_1 = Bohr radius = 0.0529 nm.

The embedded-atom method allows rapid computation of the ground-state energy of a configuration of many atoms. By varying the atomic positions it is possible to search for the minimum energy. Such quantities as the lattice constants, cohesive energy, elastic constants, and surface energies could be obtained, as well as information concerning the effects of impurities and defects.

W12.3 Peierls Instability

As an example of the utility of the tight-binding method, this section is devoted to a special phenomenon that occurs when a one-dimensional metal is constructed. With the trend toward miniaturization proceeding at the pace that it is, such a situation is not out of the realm of the possible. When the Fermi surface of an electron gas approaches certain special points in the Brillouin zone, structural instabilities may result. The special points could lie at boundaries of the Brillouin zones or could lie within the zone. Peierls showed that in a one-dimensional solid, a half-filled band results in an instability that converts the metal into an insulator. The instability produces a dimerization of adjacent atoms and doubles the size of the unit cell.

The model is depicted in Fig. W12.3, where the lattice is shown before and after dimerization. The lattice will be idealized by a tight-binding model in which the atoms are connected by springs of spring constant k_s. Prior to dimerization the electronic

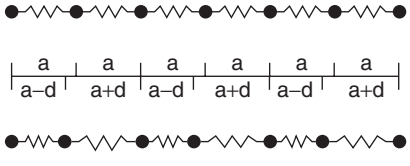

Figure W12.3. One-dimensional solid, before and after dimerization due to the Peierls instability.

energies are given by [see Eq. (7.81)]

$$E(k) = E_0 - 2t\cos ka, \tag{W12.12}$$

where E_0 is the site energy and t is the tunneling-matrix element. After dimerization two bands appear, with the respective energies

$$E_\pm = E_0 \pm \sqrt{2(t^2+\Delta^2) + 2(t^2-\Delta^2)\cos 2ka} \tag{W12.13}$$

where the tunneling-matrix elements for the springs of length $a \pm d$ have been written as $t \mp \Delta$. It is assumed that for small d the shift in Δ is proportional to d (i.e., $\Delta = \alpha d$). The lower band is occupied and the upper band is empty, so the solid becomes an insulator.

The total energy per unit length consists of the sum of the electronic energy and the elastic energy. Its change is given by

$$\frac{\delta U}{L} = \sum_s \int_{-\pi/2a}^{\pi/2a} \frac{dk}{2\pi}\left[2t\cos ka - \sqrt{2(t^2+\Delta^2) + 2(t^2-\Delta^2)\cos 2ka}\right] + \frac{k_s d^2}{2a}. \tag{W12.14}$$

The integral is expressible in terms of *E[m]*, the complete elliptic integral of the second kind,

$$\frac{\delta U}{L} \approx -\frac{2\Delta^2}{\pi at}\left(\ln\frac{4t}{\Delta} - \frac{1}{2}\right) + \frac{k_s\Delta^2}{2a\alpha^2}. \tag{W12.15}$$

For small Δ the result may be written as

$$\frac{\delta U}{L} = \frac{4t}{\pi a}\left[1 - E\left(1 - \frac{\Delta^2}{t^2}\right)\right] + \frac{k_s\Delta^2}{2a\alpha^2}. \tag{W12.16}$$

For small-enough Δ this will be negative, predicting that the instability will always occur. Minimizing δU with respect to Δ leads to

$$\Delta = 4t\exp\left[-\left(1 + \frac{\pi k_s\alpha^2 t}{4}\right)\right], \tag{W12.17}$$

with

$$\frac{\delta U}{L} = -\frac{16t}{\pi a}\exp\left[-2\left(\frac{\pi k_s\alpha^2 t}{4} + 1\right)\right]. \tag{W12.18}$$

Peierls instabilities are believed to play a role in solids constructed from linear organic molecules such as polyacetylene.

W12.4 Corrosion and Oxidation

Corrosion occurs because metals in contact with ionic solutions often function as electrodes of batteries. To see how this comes about, consider the energy needed to

extract an atom, A, from a metal in contact with a solution, and to ionize it, resulting in the ion, A^{z+}, of charge state z, and z electrons

$$A \longrightarrow A^{z+} + ze^{-}. \tag{W12.19}$$

First the cohesive energy of the atom, E_{coh}, must be provided to remove the atom from the solid into the vacuum. Then the free-space ionization energy, IE, must be added to create the ion A^{z+} in vacuum. Upon placing the charges back into solution, the solvation energy of the ion, $U_i(A^{z+})$, is regained, as well as the solvation energy of the z electrons, zU_e. Dividing this by the electronic charge, $-e$, gives a possible expression for the standard potential for the electrode half-reaction:

$$V(A \longrightarrow A^{z+} + ze^{-}) = -\frac{E_{coh} + IE - U_i(A^{z+}) - zU_e}{e}. \tag{W12.20}$$

In practice only a relative scale for the standard potential is defined. The standard potential is determined experimentally relative to a standard reaction, usually taken as that for $H_2 \rightarrow 2H^+ + 2e^-$. The standard potential V is arbitrarily defined to be zero for this reaction.

As an example of a battery, consider the Daniell cell (Fig. W12.4). Two metals, Zn and Cu, are in contact with electrolytic solutions of $ZnSO_4$ and $CuSO_4$, respectively. These metals are connected to each other electrically through some external conduction path. The electrolytes are separated from each other by a saturated salt bridge, which selectively permits passage of the SO_4^{2-} ions but blocks the passage of Cu^{2+} and Zn^{2+} ions. At the anode, Zn undergoes the oxidation reaction $Zn \rightarrow Zn^{2+} + 2e^-$, with Zn^{2+} ions going into solution and electrons going into the external circuit. The reduction reaction $Cu^{2+} + 2e^- \rightarrow Cu$ occurs at the cathode, where Cu^{2+} ions are deposited on the electrode as they recombine with circuit electrons. The net result is that the Zn corrodes and the Cu gets plated. The potential difference of this cell is computed from the difference of the standard potentials, determined by the half-reactions taking place at the electrodes:

$$Zn \longrightarrow Zn^{2+} + 2e^{-}(+0.76\ V), \qquad Cu^{2+} + 2e^{-} \longrightarrow Cu\ (-0.34\ V) \tag{W12.21}$$

and is 1.1 V. The larger this voltage, the larger the ionic current will be (according to Ohm's law), and the faster the corrosion of the Zn will be. For materials with smaller standard potential differences, the corrosion would be slower. If the sign difference

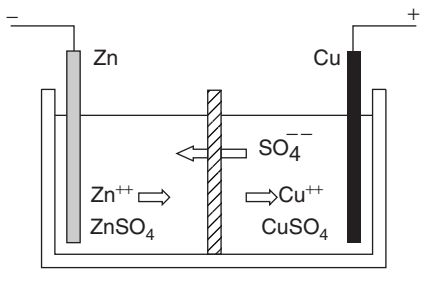

Figure W12.4. Daniell cell.

were negative instead of positive, no battery action, and consequently no corrosion, would occur. For example, if Zn were replaced by Ag, the oxidation half-reaction would be

$$2\mathrm{Ag} \longrightarrow 2\mathrm{Ag}^{+} + 2e^{-}(-1.6\ \mathrm{V}) \tag{W12.22}$$

and the standard difference would be -1.26 V, so no battery action would occur.

It is important to relate the electrode processes to the thermodynamic energies involved. The reaction $\mathrm{Cu} \rightarrow \mathrm{Cu}^{2+} + 2e^{-}$ (aqueous) involves a change of Gibbs free energy $\Delta G = -15.66$ kcal/mol $= -0.680$ eV, and the reaction $\mathrm{Zn}^{2+} + 2e^{-} \rightarrow \mathrm{Zn}$ (aqueous) has $\Delta G^0 = -35.14$ kcal/mol $= -1.525$ eV (at $T = 25^{\circ}\mathrm{C}$). The net Gibbs free energy change for the reaction is the sum of these and is -2.205 eV. Since two electrons are transferred per reaction, $z = 2$, so the open-circuit electromotive force (EMF) is $\mathscr{E}^0 = \Delta G/(-ze) = 1.10$ V. In a battery the electrical energy is supplied from the change in Gibbs free energy of the constituents.

The overall reaction for the Daniell cell may be written as $\mathrm{Zn} + \mathrm{Cu}^{2+} \rightleftharpoons \mathrm{Zn}^{2+} + \mathrm{Cu}$. For standard conditions ($T = 25^{\circ}\mathrm{C}$, $P = 1$ atm) the EMF is determined by ΔG^0. However, conditions are usually not standard and the appropriate Gibbs free energy change is

$$\Delta G = \Delta G^0 + Nk_BT \ln \frac{a_{\mathrm{Zn}^{2+}} a_{\mathrm{Cu}}}{a_{\mathrm{Cu}^{2+}} a_{\mathrm{Zn}}}, \tag{W12.23}$$

where N is the number of atoms transferred and a_i refers to the activity of species i. The EMF becomes

$$\mathscr{E} = \mathscr{E}^0 - \frac{k_BT}{ze} \ln \frac{a_{\mathrm{Zn}^{2+}}}{a_{\mathrm{Cu}^{2+}}} = \mathscr{E}^0 - \frac{k_BT}{ze} \ln \frac{a_{\mathrm{ZnSO_4}}}{a_{\mathrm{CuSO_4}}}, \tag{W12.24}$$

since $a_{\mathrm{Cu}} = a_{\mathrm{Zn}} = 1$ (by definition). Since the activities are approximately proportional to the concentrations, as the concentration of Cu^{2+} drops, so does the EMF of the cell.

It should be noted that there are similarities between electrolytic solutions and semiconductors. In the electrolyte charge is carried by the ions, whereas in the semiconductor the carriers are electrons and holes. The standard potentials of electrolytes replace the bandgap potentials of semiconductors.

Next consider a piece of iron with a drop of water on it. The outer surface of the drop is assumed to be in contact with air. Oxygen is absorbed into the water, and a concentration gradient is established with the part of the water in contact with the iron relatively deficient in oxygen. Some of the iron is oxidized and goes into solution according to the reaction

$$\mathrm{Fe} \longrightarrow \mathrm{Fe}^{2+} + 2e^{-}(+0.44\ \mathrm{V}) \tag{W12.25}$$

with the electrons entering the metal across the electrolyte–metal interface. Near the outer boundary of the water–iron interface, the oxygen is reduced by accepting the two electrons from the metal and combining with solvated protons (hydronium ions, often denoted by $\mathrm{H_3O^+}$) in solution, according to either of the two reactions

$$\begin{aligned} &\tfrac{1}{2}\mathrm{O_2} + 2\mathrm{H_3O^+} + 2e^{-} \longrightarrow 3\mathrm{H_2O}\ (+0.615\ \mathrm{V}), \\ &2\mathrm{H_3O^+} + 2e^{-} \longrightarrow 2\mathrm{H_2O} + \mathrm{H_2}\ (+1.23\ \mathrm{V}). \end{aligned} \tag{W12.26}$$

In the first case the standard potential difference is 0.175 V and in the second case it is 0.79 V. In both cases the difference is positive, so the reaction can proceed. The net result is that iron is corroded from the metal. In solution the iron ions combine with oxygen to precipitate as rust. The rust (hydrated Fe_2O_3) is deposited on the metal surface as a porous material, so additional water can come in contact with the iron.

The pH of an aqueous solution is a measure of the concentration of hydronium ions and is defined by $pH = -\log_{10} n_{H_3O^+}$, with n given in units of moles per liter (mol/L). Nernst noted that the half-potentials are dependent on the pH of the water, and shift downward with increasing pH. Thus the acidity or basicity of the electrolyte can have a strong effect on the corrosion process.

Two strategies for eliminating corrosion present themselves. One is to coat the metal with a protective overlayer and thus block ionic flow. The second is to try to alloy the metal to make its oxidation potential more negative. It is noteworthy that gold, with its standard potential for the reaction $Au \rightarrow Au^{3+} + 3e^-$ at -1.50 V, is the most negative of the elements and is therefore the most "noble" of them all. This may be understood in terms of Eq. (W12.20), because the ionization energy of Au is high (9.22 eV) and the ionic radius is large (0.137 nm), which implies that the solvation energy U_i will be small.

The extent of damage caused by corrosion is more dependent on the morphology of the oxide than on the metals themselves. It is worth contrasting the oxidation of Fe discussed above with the oxidation of Al. In the latter case the Al_2O_3 layer that is produced forms a crystal on the surface of the Al and remains in registry with the substrate. For additional oxygen atoms to come in contact with the Al, they must first diffuse through the oxide layer. Although this is possible, especially at elevated temperatures, it becomes more and more difficult as the oxide layer builds up. Thus the oxidation process becomes self-arresting. For this reason, Al_2O_3 is called a *passivation layer* in electronics application. The process of depositing such a layer, called *anodization*, is discussed further in Section 19.11. In the iron case the porous nature of the rust permits the corrosion to continue until all the iron is consumed. Chromium is added to steel to form stainless steel. A passivation layer of Cr_2O_3 is formed. It should be noted that the standard potential for the electrode reaction $Cr^{3+} + Fe = Fe^{3+} + Cr$ is -0.93 V, which is quite negative and implies that Cr_2O_3 is more likely to be produced than Fe_2O_3.

Differences in potential may exist even for a grain of single crystal between different faces, or between the surface and the interior, and these may act as the driving force for battery action and corrosion. Stress differentials across a material may also produce potential differences. This makes metals with microcracks vulnerable to corrosion.

W12.5 Coatings

The surface of a metal or alloy is often modified by applying a coating or by building the coating directly into the surface. There are numerous reasons why this is done, including enhancement of corrosion resistance (CR), wear resistance (WR), fatigue resistance (FR), oxidation resistance (OR), and thermal resistance (TR), reducing the coefficient of friction, or enabling an electric contact to be made. For example, integrated circuits based on Si have TiN and Ti deposited on them as diffusion-barrier metal films. One may also want to increase adhesion, use the surface as a catalyst, or endow the surface with special optical properties.

Traditional methods for applying coatings included such techniques as electroplating and chemical reactions. Modern materials for these coatings include SiC, TiC, TiN, TiB_2, WC, W_2C, AlN, CrN, and Si_3N_4. Coating techniques include sputtering, chemical vapor-deposition (CVD) at high temperatures (800 to 1000°C), physical vapor deposition (PVD) at lower temperatures (250 to 500°C), energetic ion implantation, and thermal reactions.

Thin coatings ($\approx$ 10 μm) of SiC, TiC, TiN, Cr_7C_3, CrN, ZrC, or ZrN are applied to tools to improve their WR and ability to cut, and where high levels of microhardness are needed. Even diamond films, the hardest substance available, and the best thermal conductor at room temperature, can be CVD-coated onto tools. The hardest coatings are made of Si_3N_4, SiC, and TiB_2.

Coatings are used in ultrahigh-vacuum systems because of their low sticking coefficients for adsorbing gases, their low yield of secondary electrons (which are ejected from a metal following the impact of a primary electron or ion), and the absence of long-lived electronic excitations, which could result in photodesorption processes. In addition, they prevent ultraclean metal parts from fusing together via the formation of diffusion bonds, in which atoms from one metal migrate over to intermediate positions between the two metals to form bridging bonds.

The coefficient of friction is often reduced substantially by applying a coating. The metals Ag, Au, or Pb may be applied to steel as a lubricant. When there is frictional heating, the coating melts and acts as a lubricant. A layer of Ti applied to steel lowers the coefficient of sliding friction. Lowering friction proves to be of considerable importance in the fabrication of semiconductors, where there are moving parts that insert, position, and remove the wafers from the vacuum system. As these parts move, there is friction. Associated with the friction is wear, and as particles are broken off, the semiconductor can become contaminated. Since liquid lubricants are of no use in a vacuum system, coatings are used instead.

There can also be improved resistance to corrosion. Typically, 50-μm layers are used. Protection is afforded by such coatings as alumina, NiCr, SiC, and CoCr. Chromium, Ni, Ta, and Ti are applied to steel and Pd or Pt are applied to Ti for this purpose. A combination of Co, Cr, Al, and Y is applied to Ni alloys. The CR is due, in part, to the dense granular structure, which tends to be equiaxed (hexagonally tiled). This presents to the surrounding electrolytic medium a material of uniform electronegativity. It also serves as an obstacle for diffusion of oxygen into grain boundary channels in the underlying metal. Yttrium coated on steel or Cr on Cu inhibits oxidation, and ZrO_2 improves the OR of Ni alloys.

Ion implantation produces a high density of interstitials, dislocations, and other defects near the surface which can act as traps for other dislocations and therefore harden the material and improve the WR. The compounds BN, CrN, SiC, Si_3N_4, TiC, TiN, ZrC, and ZrN are used to harden steels.

Electrical contacts may be deposited on Si using Ag, Al, Pt, or Au coatings. For GaAs, Al coatings may be employed, and for alumina, Cu coatings are used. The formation of silicides of Pt, Pd, and Ti on Si creates Schottky barriers, which serve as rectifiers with small forward-biased impedance.

An alloy of Co, Ni, Cr, Al, and Y acts to provide a high degree of OR for use in such applications as jet turbines. Thermal-insulation layers are often used in conjunction with these, in which case they are called thermal-barrier coatings. The goal is

to achieve low thermal diffusivity ($\kappa/\rho c_p$). Materials for TR include MgO, Y_2O_3, and ZrO_2, which have low thermal conductivities and moderate heat capacities and densities.

W12.6 Shape-Memory Alloys

It is possible to start with a hot metallic object of a particular shape, cool it, distort it, and remove the external stress, to produce what will appear to be a plastically deformed object. At a later time, however, the object may be reheated and it will return to its original shape. The ability to revert to the original shape provides the name for this class of metals — shape-memory alloys (SMA). Underlying this "talent" lies some interesting physics. Typical SMA materials include the alloys FePt, FeNiC, NiFeAlB, AuCd, NiAl, NiTi, and CuZnAl. There are also SMA materials composed of ceramic materials (e.g., PbLaZrTiO).

The SM alloys are ordered and exist in two crystalline phases. The low-temperature phase is called *martensite* (M) and the high-temperature phase is called *austenite* (A). These names stem from the nomenclature used in steel metallurgy. More generally, the high-T phase may be called the *parent phase* and the low-T phase the *daughter phase*, although here the symbols A and M are used. Phase A has a higher degree of symmetry than phase M. There is a phase transition governing the A $\leftrightarrow$ M transformation (from A to M, and vice versa). This is illustrated in Fig. W12.5, where the volume is plotted against temperature. Plots of other physical quantities, such as electrical resistance, are similar in structure and show hysterisis. Suppose that one starts in the M phase and heats the sample. At a temperature T_{A_s}, one begins to form some austenite. The amount of A formed depends on $T - T_{A_s}$. At temperature T_{A_f}, one will have reached 100% A. Above that temperature the A material is simply heated. If one then cools the sample, at a temperature T_{M_s}, one begins creating the M phase. At temperature T_{M_f}, this conversion is complete, and below T_{M_f} there is 100% M. Note the presence of a small hysteresis loop. Typical values of these temperatures for some SMA materials are given in Table W12.2.

Figure W12.6 shows the A and M phase unit cells for the NiAl intermetallic compound. The A phase has the higher-symmetry CsCl structure, while the M phase has the lower-symmetry tetragonal structure (four atoms per unit cell). The phase

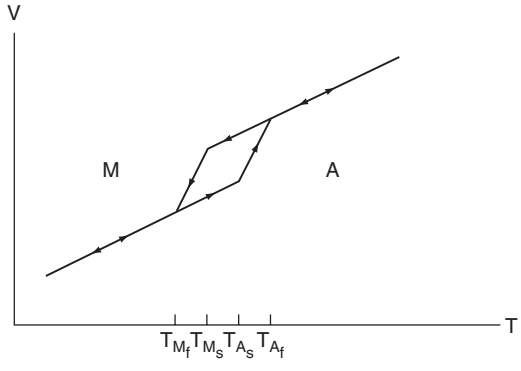

Figure W12.5. Variation of volume with temperature for a shape-memory alloy. Various critical temperatures described in the text are indicated.

TABLE W12.2 Start and Finish Temperatures for the Austenite (A) and Martensite (M) Phases of Some Shape-Memory Alloys

Shape-Memory Alloy	Temperature (°C)			
	T_{A_s}	T_{A_f}	T_{M_s}	T_{M_f}
$Au_{49.5}Cd_{50.5}$	40	42	37	35
$Zn_{25.75}Al_{4.01}Cu_{70.24}$	20	45	30	−5
$Zn_{25.60}Al_{3.90}Cu_{70.50}$	78	90	83	62
$Al_{23.9}Ni_{4.2}Cu_{71.9}$	35	80	71	26
$Ni_{58.9}Fe_{13.98}Al_{26.95}B_{0.17}$	93	172	127	56
$Ti_{50}Pd_{22}Ni_{28}$	201	252	200	107

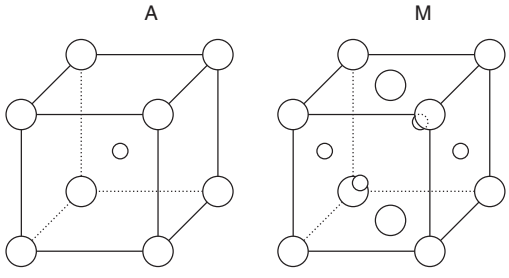

Figure W12.6. Example of the austenite and martensite unit cells in NiAl alloys.

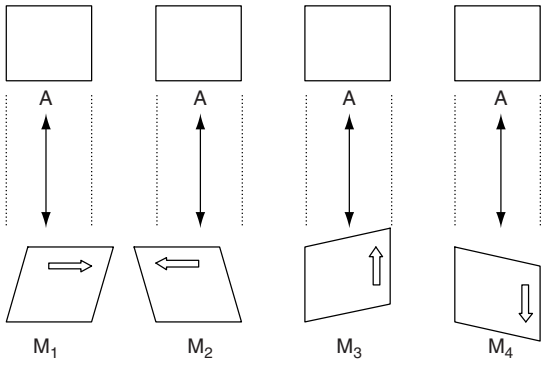

Figure W12.7. Four possible distortions of a square (phase A) to a rhombus (phase M).

transformation is reversible and is first order. No atomic-scale diffusion is taking place and no slippage of atomic planes is occurring. Everything about the transition is predictable, with randomness playing little role other than accelerating thermally assisted transitions. The material is said to be *thermoelastic*. In reality, the unit cell for the SMA materials is much larger, as may be seen by looking at the stoichiometry of the materials (see Table W12.2). It is useful to think of the unit cell as being composed of subunit cells with vacancies that may appear on different faces.

When the martensitic transition occurs, upon cooling there are a number of different states the subunits can assume in the low-symmetry phase. This is illustrated in Fig. W12.7, where the A phase is represented by a square and the M phase is

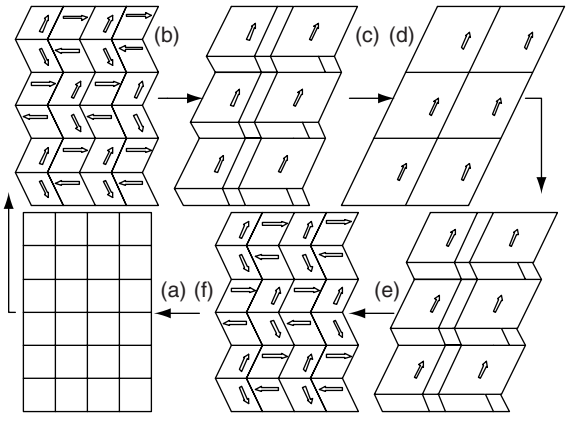

Figure W12.8. Stages in the shape-memory process.

represented by a rhombus (which has lower symmetry). The four orientations are labeled by a set of arrows. These structures self-accommodate (i.e., when the A-to-M transition occurs, there is no change in the macroscopic size of the object). The material consists of the various types of rhombi intermeshed with each other. This is illustrated in Fig. W12.8, where several such rhombi are drawn. In Fig. W12.8*a* one starts with an austenite crystal at a temperature above T_{A_f}, represented by a rectangle. The crystal is then cooled to the martensite phase. Figure W12.8*b* shows that the large-scale shape is still rectangular but now has rhombus "domains" that accommodate each other. A stress is then applied to the crystal to change its shape to a parallelogram. Figure W12.8*c* shows that one type of domain grows at the expense of the others, and eventually, in Fig. W12.8*d* the desired shape is obtained. If the stress is removed, the parallelogram shape is retained.

When a rhombus is forced to have a different orientation than its state of minimum free energy would allow, stress is built into it. The system adjusts in such a manner as to relieve this stress. This determines which rhombus will be the next to alter its shape. Modification of the structure takes place in a sequential manner. In this way the system has a memory, which consists of the sequence of stress-relaxing deformations that take place. In some ways the process is similar to magnetizing a ferromagnet, with a self-consistent strain replacing the role played by the self-consistent magnetic field. Unlike the magnetic case, however, there is only one return path that the alloy can follow when it is heated, and that is determined by the original orientations of the rhombi.

Now the sample is heated. The domains retrace their evolution (see Fig. W12.8*e* and *f*) until, when T_{A_f} is passed, the crystal has reverted to its original shape. If the temperature is lowered again, the parallelogram shape is not regained unless it is reshaped by external forces.

SMA materials exhibit a high degree of strain recovery, meaning that they revert to their original size and shape when the stress causing the strain is relaxed. For example, a NiAl alloy can have a strain recovery of 7%. The stress–strain curve exhibits superelasticity. What appears to be plastic deformation in the M phase disappears when the sample is heated to the A phase. In addition, it is possible to induce the martensitic transformation by applying an external stress field. A more complete description of the

material involves a three-dimensional phase diagram with stress plotted as a function of both strain and temperature.

Applications of SMA materials benefit from their ability to store a large amount of mechanical strain or elastic energy in a small volume. They may be used for such diverse applications as circuit breakers, switches, automatic window openers, steam-release valves, hydraulic controls for aircraft, rock cracking, sealing rings, and actuators. They can even be used to unfurl antennas on satellites, where a bulky motor assembly may be replaced by a simple SMA. A limitation on their use, however, is their slow response time, being limited by thermal conduction.

W12.7 Metallic Glasses

If a liquid metal alloy were to be rapidly quenched (i.e., its temperature lowered sufficiently rapidly) it is possible to solidify it without forming a crystalline state. Such a material is called a *metallic glass*. Since the thermal conductivity of metals is high and since the crystalline state is generally the state of lower free-energy, metals have a strong tendency to crystallize quickly. However, if a small droplet of liquid alloy is projected onto a cold surface, the resulting "splat" can cool very rapidly (with rates on the order of -10^6 K/s) and become a metallic glass. Alternatively, one could inject a fine stream of the molten alloy into a high-conductivity cold liquid to form the glass, or vapor-deposit onto a cryogenic substrate. In many ways the formation of a metallic glass is similar to that of window glass, but the thermal relaxation times are orders of magnitude faster. The metallic glasses are essentially solids, with diffusion rates often less than 10^{-22} m^2/s, orders of magnitude smaller than in crystals. The random close-packing model for metallic glasses is discussed in Chapter 4. Rapid quenching is described further in Chapter W21.

These materials are amorphous and hence do not have dislocations, but rather, a high degree of disorder on the atomic scale. They are strong, stiff, and ductile. In addition, they are corrosion resistant. Furthermore, being largely homogeneous, they allow sound to propagate without appreciable attenuation due to scattering. This is because, for most acoustic applications, the wavelength of sound is long compared with the scale size of the inhomogeneities, and the sound propagates through an effectively isotropic medium. Things are different, however, when short-wavelength phonons are involved, such as in the thermal-conduction process. Due to the lack of a crystal lattice the metallic glasses are generally poor thermal and electrical conductors, with very short phonon and electron collisional mean free paths.

Examples of metallic glasses include AuSi near the eutectic composition of 19 at % Si, $Pd_{80}Si_{20}$, $Pd_{78}Si_{16}Cu_6$, and $Ni_{36}Fe_{32}Cr_{14}P_{12}B_6$. They include transition metals (Co, Fe, La, Mn, Ni, Pd, Pt, Zr) alloyed with (B, C, N, P, Si) near the eutectic composition. Some are ferromagnetic (e.g., $Pd_{68}Co_{12}Si_{20}$ or $Fe_{83}P_{10}C_7$) and some are antiferromagnetic (e.g., $Mn_{75}P_{15}C_{10}$). The ferromagnets are readily magnetized or demagnetized, since there are no large-scale defects that pin the domain walls. The magnets are soft in the amorphous state because the domain wall thickness is much larger than the domain size. This is likely to be due to the absence of well-defined magnetic anisotropy in the magnetic metallic glass as a result of the lack of crystalline order. As discussed in Section 17.2 strong magnetic anisotropy favors magnetic domains with narrow domain walls. The metallic glass $Fe_{80}B_{11}Si_9$ is commonly used in power magnetic applications such as power distribution due to its high Curie temperature, $T_C = 665$ K, and hence its good thermal stability.

It is found that the more elements present in the alloy, the more complex the unit cell of a crystal is, and hence the longer it would take to crystallize. An example is the alloy $Zr_{41.2}Ti_{13.8}Cu_{12.5}Ni_{10.0}Be_{22.5}$ which forms a metallic glass at cooling rates of only 10 K/s. The high resistance to crystallization is believed to be due to the low melting point of the corresponding crystalline alloy and the fact that the alloy is composed of atoms of quite different sizes. Since one wants the glass to form rather than the crystal, it is preferable to work with materials with long crystallization times. This accounts for the high integers in the stoichiometry.

A further aid in the formation of the metallic glass is to have a composition corresponding to the eutectic point, as in the case of AuSi, whose binary phase diagram is sketched in Fig. W12.9. Since the eutectic temperature is low, diffusion will be sluggish when the solid is formed, and the formation of crystals will be slow. If the temperature drop is sufficiently fast, the eutectic metal will become a glass.

The metallic glass is only slightly less dense than the corresponding crystal. It tends to form a random close-packed structure (see Chapter 4) of a binary system with two sphere sizes (Fig. W12.10). The bonding is primarily metallic. There is some evidence of short-range order [i.e., there are different polyhedral arrangements (e.g., tetrahedra, octahedra, trigonal prisms and cubic biprisms)], which appear in definite proportions but are not spatially ordered. The bulk modulus of a metallic glass is found to be comparable to its crystalline counterpart. The shear modulus, however, is typically reduced by 25%. They have fairly low values of yield stress and can undergo large plastic deformations of up to about 50%. If a crack were to form and stress were concentrated in the neighborhood of its tip, the tip region would yield, the sharpness of the tip would be reduced, and the stress would be relieved. This healing mechanism curtails crack propagation and makes the material tough (i.e., able to withstand large stresses without fracturing). Repetitive cycling of the stress on and off does not work-harden the material, since no dislocations are present.

As the temperature is raised from room temperature to about half the melting temperature, activated hopping of atoms becomes important. The atoms can search for the lowest free-energy state and the solid can begin to crystallize. This prevents the metallic glasses from being employed in high-temperature applications.

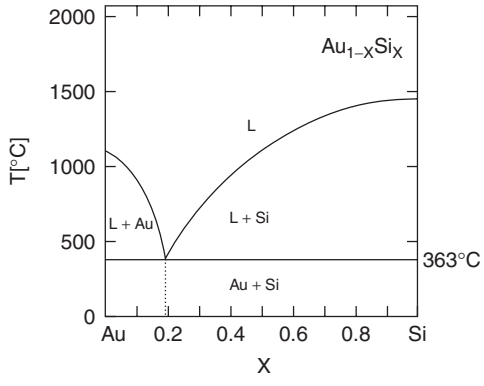

Figure W12.9. AuSi tends to form a metallic glass near the eutectic composition, indicated by the dashed line on the binary phase diagram. [Adapted from J. J. Gilman, Metallic glasses, *Phys. Today*, May 1975, p. 46. See also H. Okamoto et al., *Bull. Alloy Phase Diagrams*, **4**, 190 (1983).]

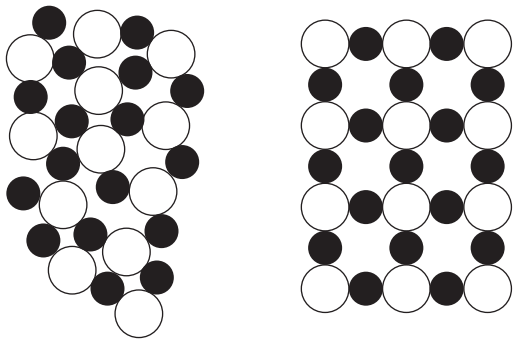

Figure W12.10. Arrangement of a binary-alloy metallic glass (*a*) compared with the crystalline state (*b*).

Possible applications for metallic glasses include transformers, tape-recording heads, filaments to reinforce rubber tires, transmission belts, and tubing. Their hardness makes them suitable for cutting instruments. Their low acoustic-attenuation feature makes them appropriate for use where sound vibrations are likely to be prevalent, such as in loudspeakers.

In crystalline metals, different crystallographic faces have different work functions and hence there is a contact potential difference between them. In an ionic solution it is possible for corrosion to take place as ionic currents between the faces are established. Due to the amorphous nature of the metallic glass, there is overall isotropy, and these contact potential differences do not exist. This tends to make the metallic glasses corrosion resistant.

W12.8 Metal Hydrides

The ability of hydrogen to adsorb on metals, dissociate, diffuse into the bulk, and then form chemical compounds provides a way to store hydrogen in metals. The density of hydrogen in metals can even exceed that of liquid hydrogen. This is attractive since the process can often be reversed and the hydrogen may be released simply by warming the metal. Hydrogen is a fuel with a high energy content and produces only water vapor when it is burned. This makes it an attractive chemical-energy source for a future technology.

Some metals can store only a fraction of a hydrogen atom per metal atom (e.g., $TaH_{0.5}$), whereas others can store more (e.g., Th_4H_{15} or CeH_3). The metal Ta has a BCC crystal structure, whereas Th and Ce have FCC crystal structures. The hydrogen atom, being small, generally occupies interstitial sites, as is illustrated in Fig. W12.11. In the left diagram there is an FCC metal with a hydrogen at one of the eight tetrahedral interstitial sites per unit cell. In the right diagram the hydrogen is at one of the four octahedral interstitial sites. In some cases all the FCC interstitial sites are occupied, such as in Th_4H_{15} and CeH_3. For an FCC cell there are eight tetrahedral interstitial sites, four octahedral interstitial sites, and four atoms per unit cell. For CeH_3 it may happen that all the interstitial sites are occupied. In Th_4H_{15} there could be more than one hydrogen per site. The hydrogen atoms generally have a high diffusivity through the

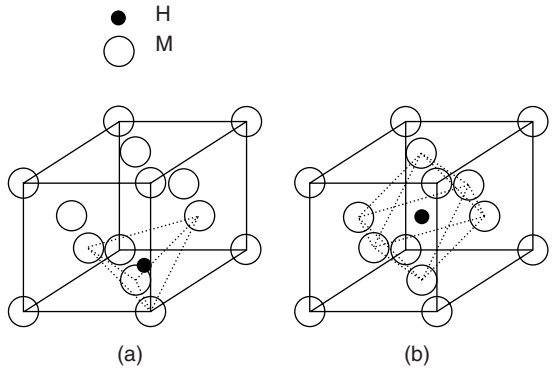

Figure W12.11. (*a*) Hydrogen at a tetrahedral interstitial site in an FCC unit cell; (*b*) hydrogen at the octahedral interstitial site in the same cell.

metal and readily hop from site to site. Some of this hopping ability is due to thermal activation, but there is also an appreciable part due to quantum-mechanical tunneling. This is similar to what occurs in the free NH_3 molecule, where the tetrahedron formed by the atoms periodically inverts as the N atom tunnels through the barrier presented by the three H atoms. (In the actual motion there is a concerted motion in which all atoms participate.) The hopping rates may be as large as a terahertz. At high-enough concentrations the absorbed hydrogen can induce structural phase transitions in the metal. This provides the means for monitoring the hydrogen content. It is also responsible for *hydrogen embrittlement*, in which a metal may be weakened by the presence of H. Imperfections, such as vacancies in the metal, can act as centers for concentrating H, and as a result, recrystallization may take place. This causes a large stress concentration and the imperfection may propagate because of it.

The presence of H may also cause drastic changes in the electrical and magnetic properties of the metal. Hydrogen generally tends to suppress magnetism. This might be expected because the origin of magnetism stems from the spin-dependent exchange interaction between neighboring metal atoms, and this, in turn, depends on the wave-function overlap. As new bonds are formed to create the hydride, less of the wave-function is left to participate in magnetism.

In some instances the H causes the metal to become a semiconductor. Electrons are extracted from the conduction band of the metal and are tied up in chemical bonds to form the hydride. It is also found that the metals may become superconductors with transition temperatures considerably higher than the bare metals, perhaps due to the enhanced electron–phonon coupling (see Chapter 16). Examples include Th_4H_{15} and PdH. Some of the anomalies observed for the hydrides are similar to those observed in the high-temperature cuprates (e.g., an absence of an isotope effect for the superconducting transition temperature).

W12.9 Solder Joints and Their Failure

Solder joints play a crucial role in the operation of electronic-circuit boards since they provide both the mechanical and, more important, the electrical connections for the various components and chips. Two modes of failure of these joints may be identified. The first is aging. In the normal course of operation the joints are subject to

thermal cycling. Due to the mismatch of coefficients of thermal expansion, heating leads to stresses. These stresses cause the motion of dislocations, which may pile up to form microscopic cracks or void spaces. The resulting embrittlement makes the joint susceptible to fracture. A second source of failure results from intermetallic compound (IMC) formation. Compound particles nucleate and grow within the joints and produce mechanical stresses due to lattice-constant mismatch, and these can also cause embrittlement. Since a typical circuit board may contain many hundreds of joints, even a small probability for failure in a joint may compound to a severe lifetime limitation for the board. The processes responsible for failure are identified by examining the joints under high-power optical microscopes.

Examples of IMC formation that results from use of the common eutectic Pb–Sn solder (see Fig. 6.8) on copper are $\mathrm{Sn} + 3\mathrm{Cu} \rightarrow \mathrm{Cu_3Sn}$ or $6\mathrm{Cu} + 5\mathrm{Sn} \rightarrow \mathrm{Cu_6Sn_5}$. Similarly, Ni can form a highly brittle compound when reacting with solder. The growth of the layer thickness of an IMC, z, is governed by an empirical equation of the form

$$\frac{dz}{dt} = A_0 \frac{e^{-E_a/k_B T}}{z^n}, \tag{W12.27}$$

where A_0 is a constant, E_a an activation energy, and n an empirical exponent ranging from $\frac{1}{2}$ to 1. It is found that the thicker the IMC layer, the more susceptible it is to brittle fracture.

Ideally, solder joints should be designed to eliminate, or at least minimize, these problems. One might try using spring-shaped elastic-component leads to relieve the thermal stresses that develop. This conflicts with the desire for a higher concentration of components on the board. It is better to match the coefficients of thermal expansion to eliminate the thermal stresses altogether. However, this often leads to a degradation of the electrical properties of the leads. It was found that decreasing the solder-joint thickness results in a reduced tendency for fractures to occur. This may be because of the ability of the joint to anneal its defects to the surface. One may also try to make the material more homogeneous so that dislocations are less likely to be present. Alternatively, one may try to alloy the material and insert dopants that would trap the dislocations and prevent them from propagating to form cracks.

To date there is no preferred method. Each has its benefits and its drawbacks. The design of joints is still in the "arts" stage.

W12.10 Porous Metals

Porous metals define a class of materials that find application in such diverse areas as filters, heat exchangers, mufflers and other noise-abatement devices, fuel cells, electrolytic cells, hydrogen-storage media, and thermal insulators. They may be fabricated using several techniques, including sintering and slip-casting. The sintering method involves mixing powders of the metal, M, with powders of another material, A, with a higher melting point. When the metal M melts, it flows around the particles of A and forms a solid metallic cage as it is cooled. If the pores are interconnected, material A can then be removed by chemical means, so the porous metal M remains. In the slip-casting method a solid foam is created from a nonmetallic material, and a dispersion of fine metal powder is absorbed by this sponge. When heated, the metal particles fuse together and the nonmetallic powder is burned away. Again the metallic foam

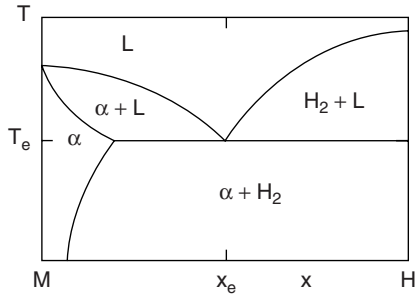

Figure W12.12. Binary phase diagram for a metal–hydrogen alloy. (Adapted from V. Shapovalov, Porous metals, *Mater. Res. Soc. Bull.*, Apr. 1994, p. 24.)

is produced. Chemical vapor-deposition techniques may be employed to build up a thickness of metal on a porous substrate and then to remove the substrate by chemical or thermal means, leaving behind a metal film.

The materials are characterized by a filling factor, which tells what fractional volume of space is occupied by the metal, a distribution of pore sizes and shapes, and a topology describing the interconnection between the pores. They are found to be poor electrical conductors, both because of the low filling factors and the high degree of boundary scattering along the thin conducting paths.

The term *gasar* has been coined to describe a foam produced by a gas–metal eutectic transition. Due to the small size of the hydrogen atom (especially when it is ionized to a proton), it has little difficulty being adsorbed in many metals, as discussed in Section W12.8. The resulting hydrogen–metal alloy phase diagram often has a eutectic transition. Such a diagram is illustrated in Fig. W12.12. The compound is of the form $M_{1-x}H_x$. Hydrogen is bubbled into the liquid metal to increase x to the eutectic composition x_e. The material is then cooled below the eutectic temperature T_e. This produces a eutectic composition consisting of a mixture of the α phase of the metallic hydride and H_2 gas. The gas is able to desorb from the hydride, leaving behind a porous structure. Gasars have proven to be the strongest of the porous–metal structures. This is probably due to a homogeneous pore size distribution, which permits loading stresses to be distributed uniformly. If residual hydrogen is trapped in the metal, the gasar is found to be a good thermal conductor, since hydrogen is light and mobile and therefore is able to convect the heat through the pore structure. The material is also able to damp acoustic waves efficiently, since the trapped gas makes inelastic collisions with the surrounding cage as the cage vibrates back and forth.

REFERENCES

Frear, D. R., and F. G. Yost, Reliability of solder joints, *Mater. Res. Soc. Bull.*, Dec. 1993, p. 49.

Gilman, J. J., Metallic glasses, *Phys. Today*, May 1975, p. 46.

Kohn, W., Overview of density functional theory, in E. K. U. Gross and R. M. Dreizler, eds., *Density Functional Theory*, Plenum Press, New York, 1995.

Shapovalov, V., Porous metals, *Mater. Res. Soc. Bull.*, Apr. 1994, p. 24.

Smith, W. F., *Structure and Properties of Engineering Alloys*, 2nd ed., McGraw-Hill, New York, 1993.

Tien, J. K., and T. Caulfield, *Superalloys, Supercomposites and Superceramics*, Academic Press, San Diego, Calif., 1994.

Wayman, C. M., Shape memory alloys, *Mater. Res. Soc. Bull.*, Apr. 1993, p. 42.

Westbrook, J. H., et al., Applications of intermetallic compounds, *Mater. Res. Soc. Bull.*, May 1996, p. 26.

Westlake, D. G., et al., Hydrogen in metals, *Phys. Today*, Nov. 1978, p. 32.